# Measurements of branching fractions and CP asymmetries in the doubly Cabibbo-suppressed decay modes $B^{\pm} \to D^0 h^{\pm}$ on 5 fb$^{-1}$

The CDF II Collaboration
*URL http://www-cdf.fnal.gov*
(Dated: November 1, 2010)

The branching fractions and CP asymmetries of $B^- \to D^0 K^-$ modes allow a theoretically-clean way of measuring the CKM angle $\gamma$. The "ADS method"[1][2] makes use of modes where the $D^0$ decays in a doubly Cabibbo-suppressed (DCS) channel: $D^0 \to K^+\pi^-$. This is a powerful method, but the corresponding decay is very rare, with a $\mathcal{BR}$ less then $2.8 \cdot 10^{-7}$ [3], and a large background is present.

Using a sample of about 5 fb$^{-1}$ of data, we reconstruct the $B \to D^0_{DCS} K$ signal and we perform a measurement of the direct CP asymmetry for the DCS modes $B^{\pm} \to D^0 \pi^{\pm}$ and $B^{\pm} \to D^0 K^{\pm}$.

We obtain, for the usual ADS parameters (definitions in the text):

$$R_{ADS}(\pi) = (4.1 \pm 0.8(stat.) \pm 0.4(syst.)) \cdot 10^{-3}$$

$$R_{ADS}(K) = (22.5 \pm 8.4(stat.) \pm 7.9(syst.)) \cdot 10^{-3}$$

$$A_{ADS}(\pi) = 0.22 \pm 0.18(stat.) \pm 0.06(syst.)$$

$$A_{ADS}(K) = -0.63 \pm 0.40(stat.) \pm 0.23(syst.)$$

This is the first measurement of these quantities at a hadron collider and the results are in agreement and competitive with measurements from other experiments.

## I. INTRODUCTION

The partial widths of $B^- \to D^0 K^-$ modes allow a thoretically-clean extraction of the CKM [4, 5] angle $\gamma = arg(-V_{ud}V_{ub}^*/V_{cd}V_{cb}^*)$ by a variety of methods, depending on the specific $D^0$ decay channel involved [1, 2, 6–8].

The precision of current experimental data [9] is still far from theoretical uncertainties and is statistics–limited, so the current knowledge of $\gamma$ can be significantly improved by the addition of further data.

All mentioned methods for extracting $\gamma$ from $B^- \to D^0 K^-$ modes require no tagging or time-dependent measurements, and many of them only involve charged particles in the final state. They are therefore particularly well–suited to analysis in a hadron collider environment, where the large production can be well exploited.

In this note we describe the reconstruction and analysis of modes where the $D^0$ decays to either $K^-\pi^+$ (Cabibbo-favored mode, CF) or $K^+\pi^-$ (doubly Cabibbo-suppressed mode, DCS). These modes allow measuring the following useful parameters for the determination of angle $\gamma$ ("ADS method" [1, 2]):

$$R_{ADS} = \frac{\mathcal{BR}(B^- \to [K^+\pi^-]_{D^0} K^-) + \mathcal{BR}(B^+ \to [K^-\pi^+]_{D^0} K^+)}{\mathcal{BR}(B^- \to [K^-\pi^+]_{D^0} K^-) + \mathcal{BR}(B^+ \to [K^+\pi^-]_{D^0} K^+)} \quad (1)$$

$$A_{ADS} = \frac{\mathcal{BR}(B^- \to [K^+\pi^-]_{D^0} K^-) - \mathcal{BR}(B^+ \to [K^-\pi^+]_{D^0} K^+)}{\mathcal{BR}(B^- \to [K^+\pi^-]_{D^0} K^-) + \mathcal{BR}(B^+ \to [K^-\pi^+]_{D^0} K^+)}. \quad (2)$$

$A_{ADS}$ and $R_{ADS}$ are related to the angle $\gamma$ through these relations:

$$R_{ADS} = r_D^2 + r_B^2 + 2 r_D r_B \cos\gamma \cos(\delta_B + \delta_D) \quad (3)$$

$$A_{ADS} = 2 r_B r_D \sin\gamma \sin(\delta_B + \delta_D)/R_{ADS} \quad (4)$$

where $r_B = |A(b \to u)/A(b \to c)|$, $\delta_B = arg[A(b \to u)/A(b \to c)]$, $r_D$ and $\delta_D$ are the corresponding amplitude ratio and strong phase difference of the $D$ meson decay amplitudes

We also measure $R_{ADS}$ and $A_{ADS}$ for the $B \to D^0\pi$ decay mode. As can be seen from the expression (4), the maximum size of the asymmetry, for given values of $r_B$ and $r_D$, is given by: $A_{ADS}(max) = 2r_B r_D/(r_B^2 + r_D^2)$ [9]. Using $r_B(\pi) \sim 0.01$, a maximum value for the asymmetry of the $\pi$ mode of about 30% can be achieved, while for the $K$ mode, using $r_B(K) \sim 0.1$, we can have a maximum value of the asymmetry of about 90%.

We reconstruct and separate the relevant modes for this analysis using a simultaneous Likelihood fit, exploiting mass and particle identification information provided by the specific ionization (dE/dx) in the CDF central drift chamber.

## II. DETECTOR AND TRIGGER

The CDF II detector [10] is a magnetic spectrometer surrounded by calorimeters and muon detectors. It provides a determination of the decay point of particles with 15 $\mu$m resolution in the transverse plane using six layers of double-sided silicon-microstrip sensors at radii between 2.5 and 22 cm from the beam. A 96-layer drift chamber extending radially from 40 to 140 cm from the beam provides excellent momentum resolution, yielding approximately 8 MeV/$c^2$ mass resolution for two body charm decays. A three-level trigger system selects events enriched in decays of long-lived particles by exploiting the presence of displaced tracks in the event and measuring their impact parameter with o?ine-like 30 $\mu$m resolution. The trigger requires presence of two charged particles with transverse momenta greater than 2 GeV/$c$, impact parameters greater than 100 microns and basic cuts on azimuthal separation and scalar sum of momenta.

## III. DATA SAMPLE AND EVENT SELECTION

The analysis is performed on a sample collected by the CDF detector between February 2002 and June 2009, corresponding to an integrated luminosity of $\sim 5$ fb$^{-1}$. The trigger is based on precision track impact parameters measured by SVT [11], and is designed to select hadronic B meson decays by requiring the presence of at least two charged particles with significant impact parameters with respect to the interaction region.

Candidates for modes $B^- \to D^0\pi^-$ with $D^0 \to K^-\pi^+$ (CF mode) and the $B^- \to D^0\pi^-$ with $D^0 \to K^+\pi^-$ (DCS mode) were reconstructed from a sample collected with the request of at least two tracks with $p_T > 2$ GeV/c, 120 $\mu$m $< |d_0| <$ 1 mm and $\Delta\Phi \leq 90^\circ$ ($\Delta\Phi$ is the transverse opening-angle between tracks). Either the two tracks from the $D^0$, or one track from the $D^0$ and one from the B may satisfy the trigger requirements.

Candidates for each particle decay tree are reconstructed according to a *bottom−up* strategy. This means that, for example, in the case of $B^- \to D^0\pi^-$, with $D^0 \to K^-\pi^+$, at first we look for a track pair vertex that is compatible with a $D^0$ decay with an invariant mass of the track pair required to lie in a mass range centered in the $D^0$ mass. This, typically, suppresses the combinatorial background. We then combine the given $D$ candidate with an additional charged track (new vertex) to reconstruct a new candidate compatible with a $B^- \to D^0\pi^-$ decay. The tracks are fitted to a secondary vertex by applying mass and pointing constraints, at the same time they are forced to comply with the proper vertex topology.

The invariant mass distributions of CF and DCS modes, with a nominal pion mass assignment to the track from B, are reported in Figs. 1 and 2, where an obvious CF signal is visible, while the DCS signal appears to be buried in the combinatorial background. Due to the smallness of the DCS Branching Ratio ($\sim 3.5 \cdot 10^{-3}$ times the CF Branching Ratio), the main issue for this analysis is the suppression of the combinatorial background.

The cuts optimization is focused on finding an evidence of the $B \to D^0_{DCS}\pi$ mode. Since the $B \to D^0_{CF}\pi$ mode has the same topology of the $DCS$ one, we performed the cuts optimization on CF mode.
We choose the $B \to D^0\pi$ signal region between $\pm 2\sigma$ around $B$ mass ($5.243\ \mathrm{GeV}/c^2 \leq M(B) \leq 5.315\ \mathrm{GeV}/c^2$), sideband subtracted, and, as background region, the mass window $5.4\ \mathrm{GeV}/c^2 \leq M(B) \leq 5.8\ \mathrm{GeV}/c^2$, where only combinatorial and no physics background appears. We maximized the figure of merit $\dfrac{S}{1.5+\sqrt{B}}$ [12], where S is the signal and B the background number of events in the CF sample.

The optimized cuts are listed in Table I.

Offline cuts on the *tridimensional vertex quality* $\chi^2_{3D}$ and on the $B$ *isolation* are very important handles to suppress combinatorial background. The B isolation variable is defined as $I = \frac{p_T(B)}{p_T(B)+\sum p_T}$, where the sum runs over all tracks contained in a cone in the $\eta$ - $\phi$ space around the B meson flight direction. We chose two cones, one at radius 1 and one at radius 0.4, because they produce a better signal-background separation than using one alone.
The *Pointing Angle* is defined as the angle between the 3-dimensional momentum of B and the 3-dimensional decay lenght. Signal events will have small pointing angles, while background events will have larger angles.
The *angular distribution of* $D^0$ is defined as the cosine of the angle between the $D^0$ in the Center of Mass frame (CM) of the B, and the flight direction of B.
The variable $\kappa$, called "kaonness", is defined as $\kappa = \dfrac{dE/dx_{meas} - dE/dx_{exp}(\pi)}{dE/dx_{exp}(K) - dE/dx_{exp}(\pi)}$, where the $dE/dx_{meas}$ is the measured specific energy loss of the particle in the drift chamber and the $dE/dx_{exp}(\pi(K))$ is the expected value for the energy lost in the drift chamber in a given particle hypothesis ($\pi(K)$), given the particle momentum. The average of $\kappa$ respectively in pion and kaon hypothesis is $< \kappa >_\pi = 0$ and $< \kappa >_K = 1$. We cut on the difference between the kaonness of the kaon from $D^0$ and of the pion from $D^0$ ($\kappa(K_D) - \kappa(\pi_D)$), to select $D^0 \to K\pi$ events rejecting $D^0 \to \pi\pi$ events.
We cut on the $D^0$ decay length measured with respect to the B decay vertex ($Lxy(D)_B$), which is not included in the optimization procedure, but its value is chosen to suppress the physics background coming from B to three body decay.
We have also three cuts on $D^0$ mass. The first is on the "correct" mass assumption of the tracks ($K\pi$) at $\pm 2\ \sigma$. This value is obtained from the cuts optimization procedure. The second is a veto cut on the "wrong" sign mass assignment ($\pi K$). For each CF and DCS event, we calculated both the correct mass and the wrong sign mass; the veto removes, in the CF sample, events peaking at the DCS mass, and in the DCS sample, events peaking at the CF mass. The third is a veto on the $D^0$ invariant mass constructed with one track from $D^0$ and the track from B. This cut ensures that CF events which can have a peaking value of the $D^0$ mass, constructed with a track from B and the kaon from $D^0$, also passing the DCS selection, are removed. The vice versa is also applied.

The resulting invariant mass distributions of $B^- \to D^0\pi^- \to [K^-\pi^+]_D\pi^-$ (CF) and $B^- \to D^0\pi^- \to [K^+\pi^-]_D\pi^-$ (DCS), with pion mass assignment to the track from B, were reported in Figs. 3 and 4.

The combinatorial background is almost reduced to zero.

## IV. SAMPLE COMPOSITION FIT

Our goal is to measure the relative yields of $B^- \to D^0_{DCS}h^-$ with respect to $B^- \to D^0_{CF}h^-$ ($h = K, \pi$) and the DCS charge asymmetries. To this purpose, we perform an unbinned maximum likelihood fit which combines invariant mass and Particle IDentification (PID) information for all modes of interest simultaneously.

Fig. 5 shows the contribution to physics background from other $B$ modes, obtained from a generic B Montecarlo sample, in the CF reconstruction. A single component dominates the background in the mass region of the $DK$ signal: the mode $B^- \to D^{0*}\pi^-$ where a soft $\gamma$ or $\pi^0$ from $D^{0*}$ decay was lost. We use, as lower mass fit limit, $5.17\ \mathrm{GeV}/c^2$ in order to ensure that contributions other than $B^- \to D^0\pi^-$ and $B^- \to D^{0*}\pi^-$ were negligible. The presence of a

pion in this background, allows exploiting the dE/dx information on the $B$ track as a handle in separating them from the $DK$ signal.

Since the combinatorial background, after the optimization, is very low, we need a sufficient lever arm to model correctly its slope and its normalization: so we choose 6.5 GeV/$c^2$ as maximum mass fit limit.

For what concern the DCS backgrounds, we find contributions coming from the following modes:

- $B^- \to D^0\pi^-$, with $D^0 \to X$;
- $B^- \to D^0K^-$, with $D^0 \to X$;
- $B^- \to K^-\pi^+\pi^-$;
- $B^0 \to D_0^{*-}e^+\nu_e$.

We perform a simultaneous fit for the two channels, the Cabibbo Favored mode ($B^- \to D^0K^- \to [K^-\pi^+]K^-$) and the Doubly Cabibbo Suppressed mode ($B^- \to D^0K^- \to [K^+\pi^-]K^-$). The structure of the Likelihood, described below, is the same for both channels.
The fraction of the physics background ($B^- \to D^{0*}\pi^-$) with respect to the $B^- \to D^0\pi^-$ signal is common to the two modes. The simultaneous fit allows us to take advantage of the higher statistics channel to constrain the common parameters in a consistent way. Also signal and background templates are common.

The discriminating observables used in the fit are the following:

- $M_{D^0\pi}$: the invariant mass assigning the pion mass at the track from $B$.
- The "kaonness" $\kappa$ which contain the dE/dx information for the track from $B$. The particle identification in the fit is used only for the track from $B$ to distinguish between $B \to DK$ and $B \to D\pi$ modes. The distribution of kaonness $\kappa$ is crosschecked with the two tracks from the $D^0$ which are unambiguosly identified from kinematics.

The expression of the Likelihood is:

$$\mathcal{L} = \mathcal{L}_{CF+} \cdot \mathcal{L}_{CF-} \cdot \mathcal{L}_{DCS+} \cdot \mathcal{L}_{DCS-} \tag{5}$$

where $\mathcal{L}_{CF+}$ and $\mathcal{L}_{CF-}$ are the components for CF sample, positive and negative charges respectively, while $\mathcal{L}_{DCS+}$ and $\mathcal{L}_{DCS-}$ are the component for DCS sample, for positive and negative charges.
They are defined as:

$$\begin{aligned}\mathcal{L}_{CF+} = \prod_i^{Nevents} \big[&(1-b_{CF+})\cdot\left(f_\pi^{CF+}\cdot pdf_\pi(M,\kappa) + \mathbf{c}^+\cdot f_\pi^{CF+}\cdot pdf_{D*}(M,\kappa) + \right.\\ &\left.+\left(1-f_\pi^{CF+}-\mathbf{c}^+\cdot f_\pi^{CF+}\right)\cdot pdf_K(M,\kappa)\right) + b_{CF+}\cdot pdf_{comb}(M,\kappa)\big]\end{aligned}$$

with a similar expression for $\mathcal{L}_{CF-}$, and:

$$\begin{aligned}\mathcal{L}_{DCS+} = \prod_i^{Nevents} \big[&(1-b_{DCS+})\cdot\left(f_\pi^{DCS+}\cdot pdf_\pi(M,\kappa) + \mathbf{c}^+\cdot f_\pi^{DCS+}\cdot pdf_{D*}(M,\kappa) + \right.\\ &\left.+\left(1-f_\pi^{DCS+}-\mathbf{c}^+\cdot f_\pi^{DCS+}\right)\cdot pdf_K(M,\kappa)\right) + \\ &+b_{DCS+}\cdot\Big(f^+_{[X]\pi}\cdot pdf_{[X]\pi}(M,\kappa) + f^+_{[X]K}\cdot pdf_{[X]K} + f^+_{K\pi\pi}\cdot pdf_{K\pi\pi}(M,\kappa) + \\ &f^+_{B^0}\cdot pdf_{B^0}(M,\kappa) + (1-f^+_{[X]\pi}-f^+_{[X]K}-f^+_{K\pi\pi}-f^+_{B^0})\cdot pdf_{comb}(M,\kappa)\Big)\big]\end{aligned}$$

with a similar expression for the $\mathcal{L}_{DCS-}$.

The parameters $b_{CF+}$, $b_{CF-}$, $b_{DCS+}$ and $b_{DCS-}$ are the fractions of the background for each mode and charge. In the CF likelihood the only background considered is the combinatorial, for which we use a single $pdf_{comb}$ for both positive and negative charges. For the DCS background we are considering the combinatorial (with the same $pdf$ of CF mode) plus $B \to K\pi\pi$ (of which the fraction is $f^\pm_{K\pi\pi}$ and the pdf is $pdf_{K\pi\pi}$), plus $B \to D^0\pi$ with $D^0 \to X$ (of which the fraction is $f^\pm_{[X]\pi}$ and the pdf is $pdf_{[X]\pi}$), plus $B \to D^0K$ with $D^0 \to X$ (of which the fraction is $f^\pm_{[X]K}$ and the pdf is $pdf_{[X]K}$), plus $B^0 \to D_0^{*-}e^+\nu_e$ (of which the fraction is $f^\pm_{B^0}$ and the pdf is $pdf_{B^0}$).

For the signal we are using the same functional expression for CF and DCS modes. $f_\pi^{CF,DCS,\pm}$ is the fraction of $B \to D^0\pi$ CF, DCS, positive and negative charges. $\mathbf{c}^\pm$ is the common parameter for CF and DCS likelihood and corresponds to the ratio between $B \to D^*\pi$ over $B \to D^0\pi$.

The fraction of $B \to D^0 K$ is written as $(1 - f_\pi - c \cdot f_\pi)$. This expression means that we measure the DK fraction starting from the $D\pi$ fraction.

The *pdf*s are functions of the Mass (M) in $D^0\pi$ hypothesis and of Particle Identification ($\kappa$). They are different for each decay, but equal in CF and DCS Likelihoods. The $pdf(\kappa)$ is obtained using a sample of kaons and pions from $D^0 \to K^-\pi^+$ decays.

We describe the shape of the combinatorial background using an exponential. We verified that this parameterization is correct in $B$ events in the $D^0$ mass sidebands. The slope of the exponential is then determined by the fit.
The PID pdf for the combinatorial background was obtained in the assumption that it is dominated by pions and kaons:

$$a \cdot pdf_\pi(\kappa) + (1 - a) \cdot pdf_K(\kappa) \tag{6}$$

where $a$ is the fraction of pions in the combinatorial background and is left free to float in the central fit.

## V. FIT RESULT

The raw number of events obtained by the maximum Likelihood fit are reported in Tables II and III for the signals, and IV and V for the backgrounds.

We report the plots of fit projections on $M_{D^0\pi}$ and $\kappa$ for the CF (Figs. 6 and 7) and DCS samples (Figs. 8 and 9). In Figs. 10 the logarithmic scale of the DCS plots shows the backgrounds contributions.

The raw fit results are then corrected for detector effects. The only correction needed by the direct CP-asymmetry $A_{ADS}(K)$ and the branching fraction $R_{ADS}(K)$ is due to different probability for $K^+$ and $K^-$ to interact with the tracker material. This effect is reproduced rather well by GEANT [14]. The asymmetry $\frac{\epsilon(K^+)}{\epsilon(K^-)} = 1.0178 \pm 0.0023(stat.) \pm 0.0045(syst.)$ [15] is estimated with a careful study on a large Monte Carlo sample. The corrected results are as follows:

$$R_{ADS}(K) = \frac{N_{raw}(B^- \to D^0_{DCS}K^-) \cdot \frac{\epsilon(K^+)}{\epsilon(K^-)} + N_{raw}(B^+ \to D^0_{DCS}K^+)}{N_{raw}(B^- \to D^0_{CF}K^-) \cdot \frac{\epsilon(K^+)}{\epsilon(K^-)} + N_{raw}(B^+ \to D^0_{CF}K^+)} = [22.5 \pm 8.4\ (stat.)] \cdot 10^{-3}. \tag{7}$$

$$A_{ADS}(K) = \frac{N_{raw}(B^- \to D^0_{DCS}K^-) \cdot \frac{\epsilon(K^+)}{\epsilon(K^-)} - N_{raw}(B^+ \to D^0_{DCS}K^+)}{N_{raw}(B^- \to D^0_{DCS}K^-) \cdot \frac{\epsilon(K^+)}{\epsilon(K^-)} + N_{raw}(B^+ \to D^0_{DCS}K^+)} = -0.63 \pm 0.40\ (stat.). \tag{8}$$

The results for the other two observables are:

$$R_{ADS}(\pi) = \frac{N_{raw}(B^- \to D^0_{DCS}\pi^-) + N_{raw}(B^+ \to D^0_{DCS}\pi^+)}{N_{raw}(B^- \to D^0_{CF}\pi^-) + N_{raw}(B^+ \to D^0_{CF}\pi^+)} = [4.1 \pm 0.8\ (stat.)] \cdot 10^{-3}. \tag{9}$$

$$A_{ADS}(\pi) = \frac{N_{raw}(B^- \to D^0_{DCS}\pi^-) - N_{raw}(B^+ \to D^0_{DCS}\pi^+)}{N_{raw}(B^- \to D^0_{DCS}\pi^-) + N_{raw}(B^+ \to D^0_{DCS}\pi^+)} = 0.22 \pm 0.18\ (stat.). \tag{10}$$

## VI. SYSTEMATICS UNCERTAINTIES

We have considered the following sources of systematics uncertanties:

- *dE/dx induced systematics.* We have repeated the fit varying the parameters of the dE/dx templates used in the fit, randomly in a $1\sigma$ and $2\sigma$-radius multidimensional sphere in the space of the parameters of dE/dx calibrations. This method is described in [16], [17], [18].

- *Combinatorial background mass model systematics.* Our central fit assumes a mass-shape of the combinatorial background events distributed as an exponential function. We verified that the shape is exponential also under the $B$ peaks, using $B$ events in the $D^0$ sidebands ($3\sigma$). We varied the fit range from $[5.17, 6.5]$ to $[5.17, 5.8]$ GeV/$c^2$.

- *Physics background mass model systematics.* We varied the shape of the physics background.
  - $B^- \to D^0\pi$ with $D^0 \to X$
    The mass shape is parametrized with a gaussian, we varied the mean and the width of $\pm 1\sigma$.
  - $B^- \to D^0 K$ with $D^0 \to X$
    We parametrized the mass shape with a gaussian, we varied the mean and the width of the gaussian of $\pm 1\sigma$.
  - $B^- \to K^-\pi^+\pi^-$
    We parametrized the mass shape with two gaussians. We varied the mean and the width of the second gaussian, that is the one goes under the B signal peaks, of $\pm 1\sigma$.
  - $B^0 \to D_0^{*-} e^+ \nu_e$
    We parametrized the mass shape with two gaussians. We varied the mean and the width of the second gaussian, that is the one goes under the B signal peaks, of $\pm 1\sigma$.
  - $B^- \to D^{*0}\pi^-$
    We parametrized the mass shape with three gaussians plus an exponential. We varied the slope of the exponential of $\pm 1\sigma$.
- *Uncertainty on the $K^-/K^+$ efficiency.* The uncertainty on the efficiency is used to evaluate a systematic error on the observables.
- *Fit bias.* We found small biases in the maximum likelihood fit. We measured these biases by repeated fits on simulated sample and we added the values as systematic errors.

A summary of all systematics is reported in Table VI. The total systematic uncertainty on each measurement is determined as the sum in quadrature of all systematic uncertainties.

## VII. RESULTS

We recontructed the DCS signals $B \to D^0\pi$ and $B \to D^0 K$ with a total significance greater than 5 $\sigma$.
Using 5 fb$^{-1}$ of data we measure:

$$R_{ADS}(\pi) = \frac{BR(B^- \to D^0_{DCS}\pi^-) + BR(B^+ \to D^0_{DCS}\pi^+)}{BR(B^- \to D^0_{CF}\pi^-) + BR(B^+ \to D^0_{CF}\pi^+)} =$$

$$= [4.1 \pm 0.8\ (stat.) \pm 0.4\ (syst.)] \cdot 10^{-3}$$

$$R_{ADS}(K) = \frac{BR(B^- \to D^0_{DCS}K^-) + BR(B^+ \to D^0_{DCS}K^+)}{BR(B^- \to D^0_{CF}K^-) + BR(B^+ \to D^0_{CF}K^+)} =$$

$$= [22.5 \pm 8.4\ (stat.) \pm 7.9\ (syst.)] \cdot 10^{-3}$$

$$A_{ADS}(\pi) = \frac{BR(B^- \to D^0_{DCS}\pi^-) - BR(B^+ \to D^0_{DCS}\pi^+)}{BR(B^- \to D^0_{DCS}\pi^-) + BR(B^+ \to D^0_{DCS}\pi^+)} =$$

$$= 0.22 \pm 0.18\ (stat.) \pm 0.06\ (syst.)$$

$$A_{ADS}(K) = \frac{BR(B^- \to D^0_{DCS}K^-) - BR(B^+ \to D^0_{DCS}K^+)}{BR(B^- \to D^0_{DCS}K^-) + BR(B^+ \to D^0_{DCS}K^+)} =$$

$$= -0.63 \pm 0.40\ (stat.) \pm 0.23\ (syst.)$$

These quantities are measured for the first time in hadron collisions. The results are in agreement with existing measurements performed at $\Upsilon(4S)$ resonance (Figs. 11-14). These measurements can be combined with other $B^- \to D^0 K^-$ decay parameters to improve the determination of CKM angle $\gamma$.

## ACKNOWLEDGMENTS

We thank the Fermilab staff and the technical staffs of the participating institutions for their vital contributions. This work was supported by the U.S. Department of Energy and National Science Foundation; the Italian Istituto Nazionale di Fisica Nucleare; the Ministry of Education, Culture, Sports, Science and Technology of Japan; the Natural Sciences and Engineering Research Council of Canada; the National Science Council of the Republic of China; the Swiss National Science Foundation; the A.P. Sloan Foundation; the Bundesministerium fuer Bildung und Forschung, Germany; the Korean Science and Engineering Foundation and the Korean Research Foundation; the Particle Physics and Astronomy Research Council and the Royal Society, UK; the Russian Foundation for Basic Research; the Comision Interministerial de Ciencia y Tecnologia, Spain; and in part by the European Community's Human Potential Programme under contract HPRN-CT-20002, Probe for New Physics.

[1] D.Atwood, I.Dunietz, A.Soni, Phys. Rev. D 63, 036005.
[2] D.Atwood, I.Dunietz, A.Soni, Phys. Rev. Lett. 78, 3257.
[3] K. Nakamura et al. (Particle Data Group), J. Phys. G 37, 075021 (2010).
[4] M. Kobayashi and T Maskawa, "CP Violation in the Renormalizable Theory of Weak Interaction", Prog. Theor. Phys., 49(2) 652-657,1973.
[5] N. Cabibbo, "Unitary Simmetry and Leptonics Decays", Phys. Rev. Lett., 10: 511-533,1963.
[6] M.Gronau, D.Wyler, Phys. Lett. B 265,172.
[7] M.Gronau, D.London, Phys. Lett. B 253,483.
[8] A.Giri, Y.Grossman, A.Soffer, J.Zupan, Phys. Rev. D 68, 054018.
[9] The Heavy Flavor Averaging Group. http://www.slac.stanford.edu/xorg/hfag/index.html
[10] F. Abe, et al., Nucl. Instrum. Methods Phys. Res. A **271**,387 (1988);D. Amidei, et al., Nucl. Instum. Methods Phys. Res. A **350**, 73 (1994);F. Abe, et al., Phys. Rev. D **52**, 4784 (1995);P. Azzi, et al., Nucl. Instrum. Methods Phys. Res. A **360**, 137 (1995);The CDF II Detector Technical Design Report, Fermilab-Pub-96/390-E.
[11] I.Furic et al., "The Silicon Vertex Trigger Upgrade at CDF" Proceedings 10th Pisa Meeting on advanced detectors, frontier detectors for frontier physics, La Biodola, Elba, Italy, May 21-27, 2006.
[12] G. Punzi, *"Sensitivity of searches for new signals and its optimization."*, arXiv:0808063v2 [physics.data-an], (2003).
[13] E.Baracchini and G.Isidori, "Electromagnetic corrections to non-leptonic two body B and D decays", Phys. Lett. B633, 309 (2006), [hep-ph/0508071].
[14] R.Brun, R.Hagelberg, M.Hansroul, and J.C.Lassalle, Reports no. CERN-DD-78-2-REV and CERN-DD-78-2.
[15] S. Giagu et al., "Relative Branching Fractions and CP-violating decay rate Asymmetries in Cabibbo suppressed decays of the $D^0$ meson" CDF-note 6391.
[16] P.Squillacioti et al., "Update of Combined PID in 5.3.4" CDF-note 7866.
[17] P.Squillacioti et al., "Update of Combined PID in 6.1.4" CDF-note 8478.
[18] http://www-cdf.fnal.gov/internal/physics/bottom/bpak/pid/CombPID_page.html

| Parameter | Value |
|---|---|
| $B$ decay length significance: $\frac{L_{xy}(B)}{\sigma_{L_{xy}(B)}}$ | $\geq 12$ |
| $B$ impact parameter: $\lvert d_0(B)\rvert$ | $\leq 0.005$ cm |
| $B$ tridimensional vertex quality: $\chi_{3D}$ | $\leq 13$ |
| $B$ Isolation (Cone 1): $Isol_1$ | $\geq 0.4$ |
| $B$ Isolation (Cone 0.4): $Isol_{0.4}$ | $\geq 0.7$ |
| $B$ pointing angle: $PA(B)$ | $\leq 0.15$ |
| $L_{xy}(D)_B$ | $\geq 0.01$ |
| $\Delta R = \sqrt{\Delta\Phi^2 + \Delta\eta^2}$ between the track from B and the $D^0$: $\Delta R$ | $\leq 1.5$ |
| $D$ angular distribution: $\lvert\cos(\theta^*_D)\rvert$ | $\leq 0.6$ |
| Difference $\kappa(K_D) - \kappa(\pi_D)$ | $\geq -1$ |
| $D^0$ mass in $K\pi$ hypothesis: | $1.8495 \leq M(D) \leq 1.8815$ |
| $D^0$ mass in $\pi K$ hypothesis: | $M(D^0_{WS}) \leq 1.8245,\ M(D^0_{WS}) \geq 1.9045$ |
| $D^0$ mass in $K\pi_B$ hypothesis: | $M(D^0_{K\pi_B}) \leq 1.8245,\ M(D^0_{K\pi_B}) \geq 1.9045$ |

TABLE I. Optimized cuts.

| Decay | yield |
|---|---|
| $B^+ \to \overline{D}^0\pi^+$ CF | $8872 \pm 103$ |
| $B^- \to D^0\pi^-$ CF | $8804 \pm 103$ |
| $B^+ \to \overline{D}^0K^+$ CF | $727 \pm 47$ |
| $B^- \to D^0K^-$ CF | $785 \pm 49$ |
| $B^+ \to \overline{D}^0\pi^+$ DCS | $29 \pm 10$ |
| $B^- \to D^0\pi^-$ DCS | $44 \pm 12$ |
| $B^+ \to \overline{D}^0K^+$ DCS | $28 \pm 11$ |
| $B^- \to D^0K^-$ DCS | $6 \pm 8$ |

TABLE II. Raw results from the maximum likelihood fit for the signal events, separated charge.

| Decay | yield |
|---|---|
| $B^+ \to \overline{D}^0\pi^+ + c.c.$ CF | $17677 \pm 146$ |
| $B^+ \to \overline{D}^0K^+ + c.c.$ CF | $1513 \pm 68$ |
| $B^+ \to \overline{D}^0\pi^+ + c.c.$ DCS | $73 \pm 16$ |
| $B^+ \to \overline{D}^0K^+ + c.c.$ DCS | $34 \pm 14$ |

TABLE III. Raw results from the maximum likelihood fit for the total signal events.

| Decay | Yield |
|---|---|
| $B^+ \to D^{0*}\pi^+$ CF | $307 \pm 30$ |
| $B^- \to \overline{D}^{0*}\pi^-$ CF | $365 \pm 33$ |
| $B^+ \to D^{0*}\pi^+$ DCS | $1 \pm 1$ |
| $B^- \to \overline{D}^{0*}\pi^-$ DCS | $2 \pm 1$ |
| $B^+ \to D^0\pi^+$ with $D^0 \to X$ | $45 \pm 9$ |
| $B^- \to D^0\pi^-$ with $D^0 \to X$ | $45 \pm 9$ |
| $B^+ \to D^0K^+$ with $D^0 \to X$ | $2 \pm 1$ |
| $B^- \to D^0K^-$ with $D^0 \to X$ | $2 \pm 2$ |
| $B^+ \to K^+\pi^-\pi^+$ | $9 \pm 3$ |
| $B^- \to K^-\pi^-\pi^+$ | $9 \pm 3$ |
| $B^0 \to D_0^{*-}e^+\nu_e$ | $2 \pm 2$ |
| $B^0 \to D_0^{*+}e^-\bar{\nu_e}$ | $2 \pm 2$ |

TABLE IV. Raw results from the maximum likelihood fit for the background events, separated charge.

| Decay | Yield |
|---|---|
| $B^+ \to D^{0*}\pi^+ + c.c$ CF | $672 \pm 45$ |
| $B^+ \to D^{0*}\pi^+ + c.c$ DCS | $3 \pm 2$ |
| $B^+ \to D^0\pi^+ + c.c$ with $D^0 \to X$ | $90 \pm 13$ |
| $B^+ \to D^0K^+ + c.c$ with $D^0 \to X$ | $4 \pm 3$ |
| $B^+ \to K^+\pi^-\pi^+ + c.c$ | $18 \pm 4$ |
| $B^0 \to D_0^{*-}e^+\nu_e + c.c$ | $4 \pm 3$ |

TABLE V. Raw results from the maximum likelihood fit for the total background events.

| **Source** | $R_{ADS}(\pi)$ | $R_{ADS}(K)$ | $A_{ADS}(\pi)$ | $A_{ADS}(K)$ |
|---|---|---|---|---|
| dE/dx | 0.0001 | 0.0050 | 0.0560 | 0.070 |
| combinatorial background | 0.0003 | 0.0037 | 0.0073 | 0.153 |
| $B^- \to [X]_D\pi^-$ shape | 0.0002 | 0.0025 | 0.0067 | 0.057 |
| $B^- \to [X]_DK^-$ shape | - | 0.0001 | 0.0003 | 0.003 |
| $B^- \to K^-\pi^+\pi^-$ shape | 0.0001 | 0.0004 | 0.0049 | 0.009 |
| $B^0 \to D_0^{*-}e^+\nu_e$ shape | - | 0.0003 | 0.0020 | 0.007 |
| $B^- \to D^{*0}\pi^-$ shape | - | 0.0005 | 0.0009 | 0.013 |
| efficiency | - | 0.0001 | - | 0.003 |
| bias | 0.0001 | 0.0042 | 0.0159 | 0.148 |
| **Total** | **0.0004** | **0.0079** | **0.059** | **0.232** |

TABLE VI. Systematics summary.

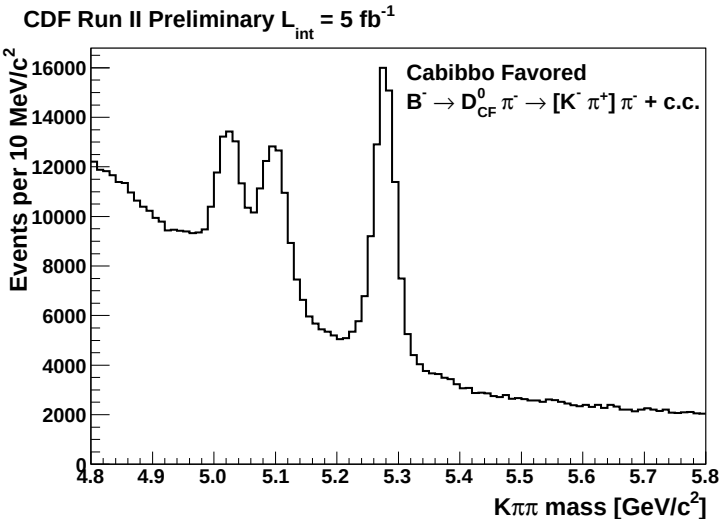


FIG. 1. Invariant mass distribution of $B^- \to D^0\pi^-$ with $D^0 \to K^-\pi^+$ (Cabibbo-favored mode) before the optimized cuts.

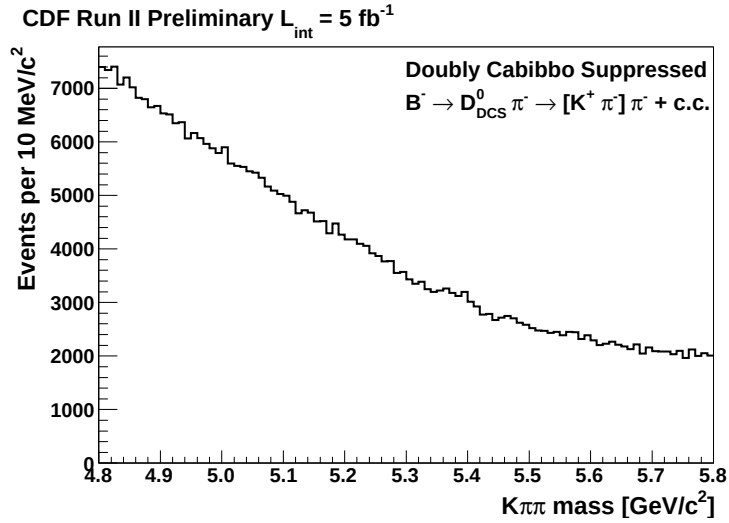


FIG. 2. Invariant mass distribution of $B^- \to D^0\pi^-$ with $D^0 \to K^+\pi^-$ (doubly Cabibbo-suppressed mode) before the optimized cuts.

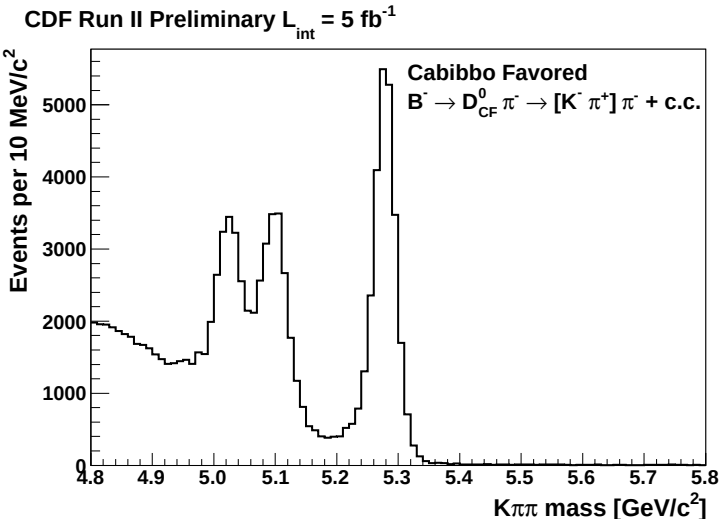


FIG. 3. Invariant mass distribution of $B^- \to D^0\pi^-$ with $D^0 \to K^-\pi^+$ (Cabibbo-favored mode) after the optimized cuts.

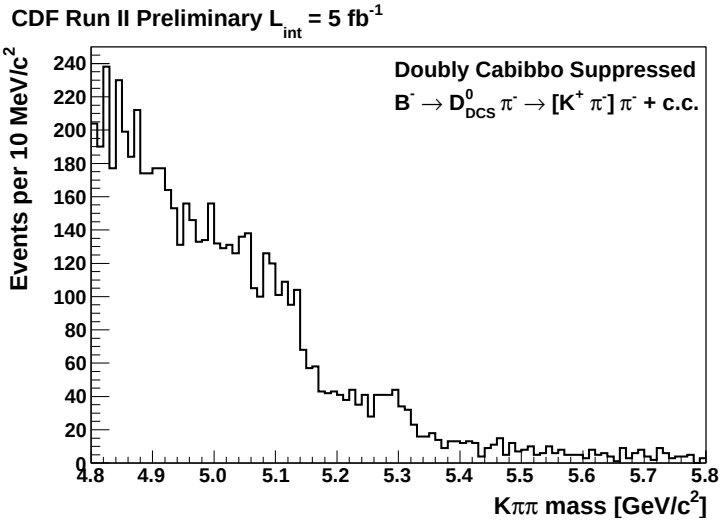


FIG. 4. Invariant mass distribution of $B^- \to D^0\pi^-$ with $D^0 \to K^+\pi^-$ (doubly Cabibbo-suppressed mode) after the optimized cuts.

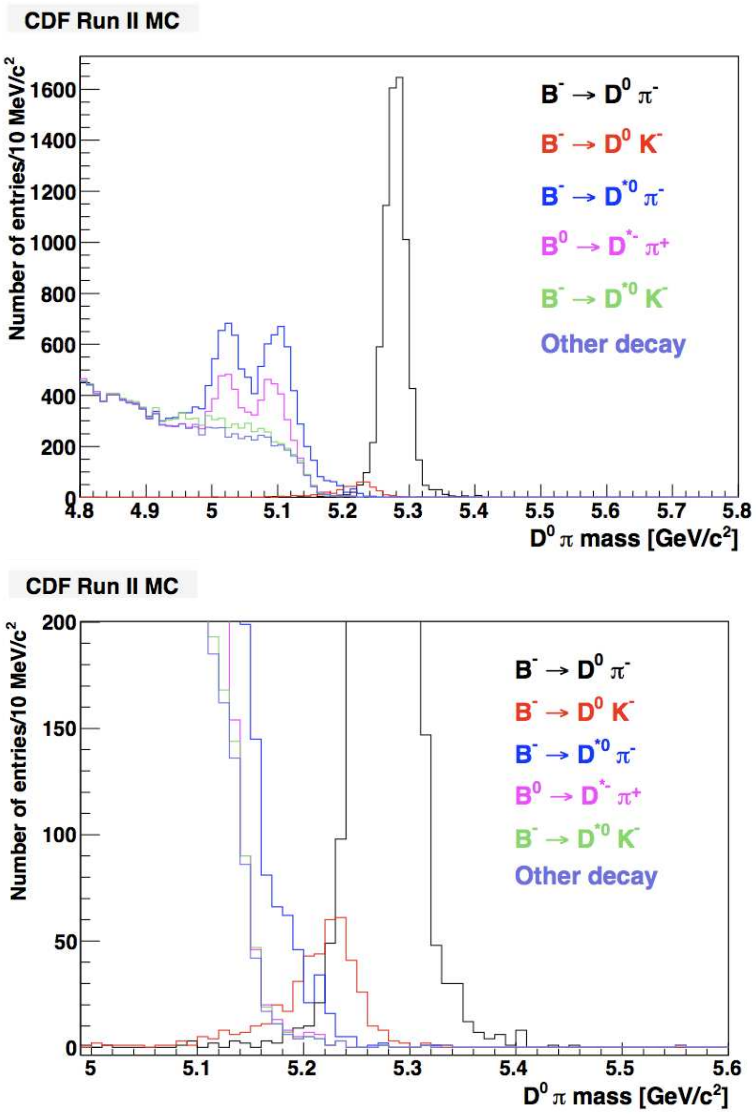


FIG. 5. Generic MC of $B^+$. On the bottom a magnification of the mass distributions to see the $B \to D^0 K$ decay.

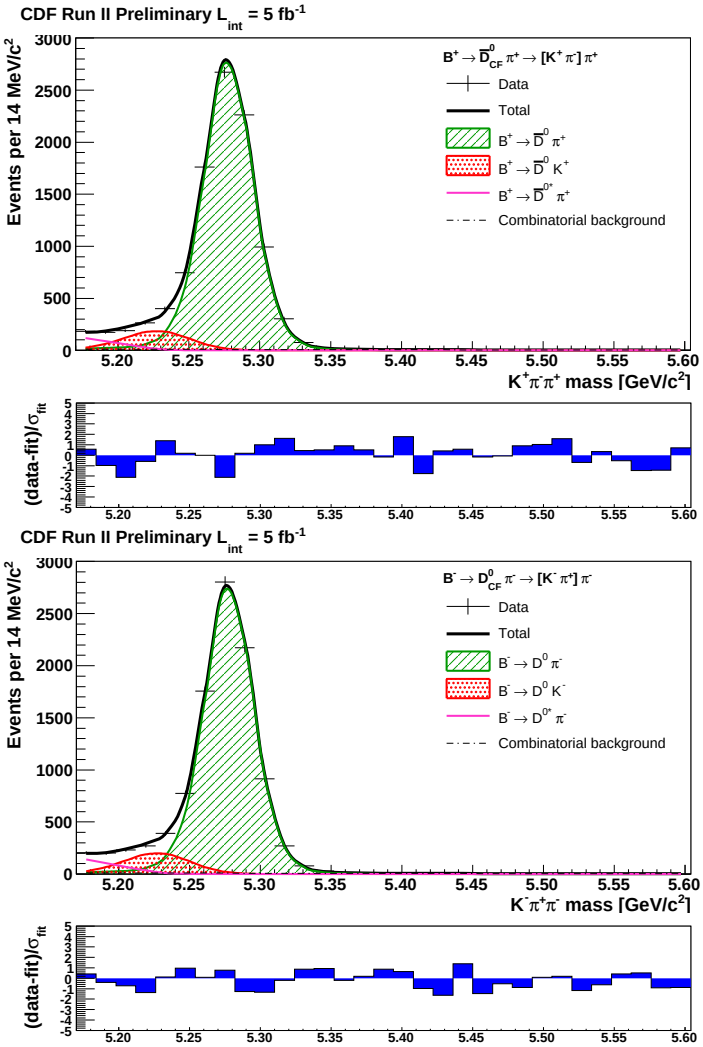


FIG. 6. Fit projection onto the $m_{D^0\pi}$ variable for the Cabibbo-favored mode, positive charges (top) and negative charges (bottom).

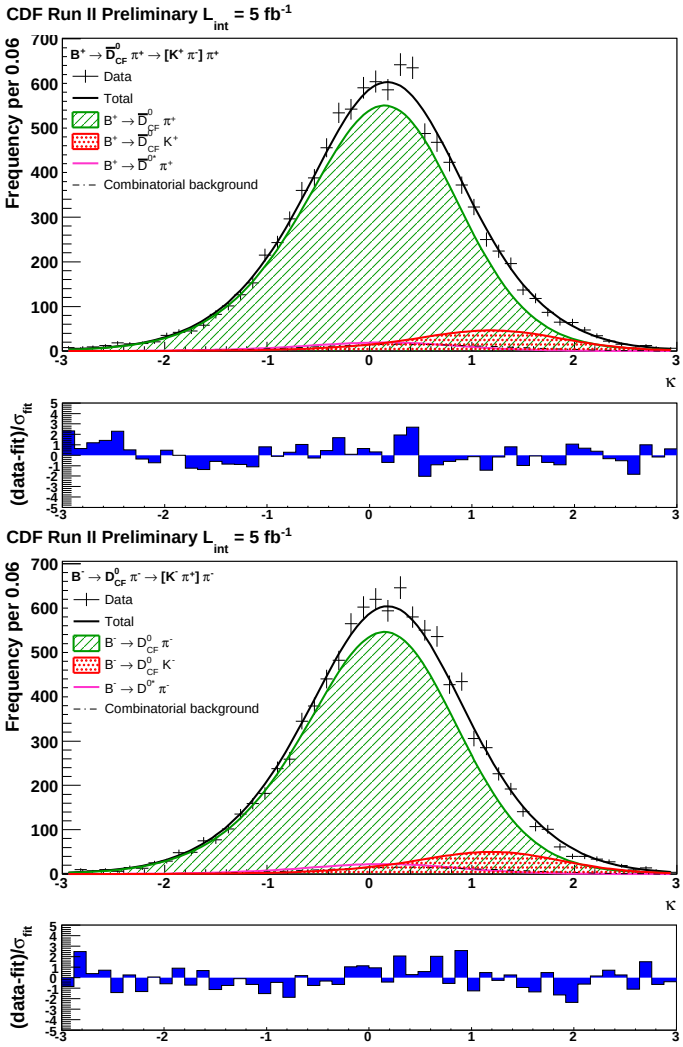


FIG. 7. Fit projection onto the $\kappa$ variable for the Cabibbo-favored mode, positive charges (top) and negative charges (bottom).

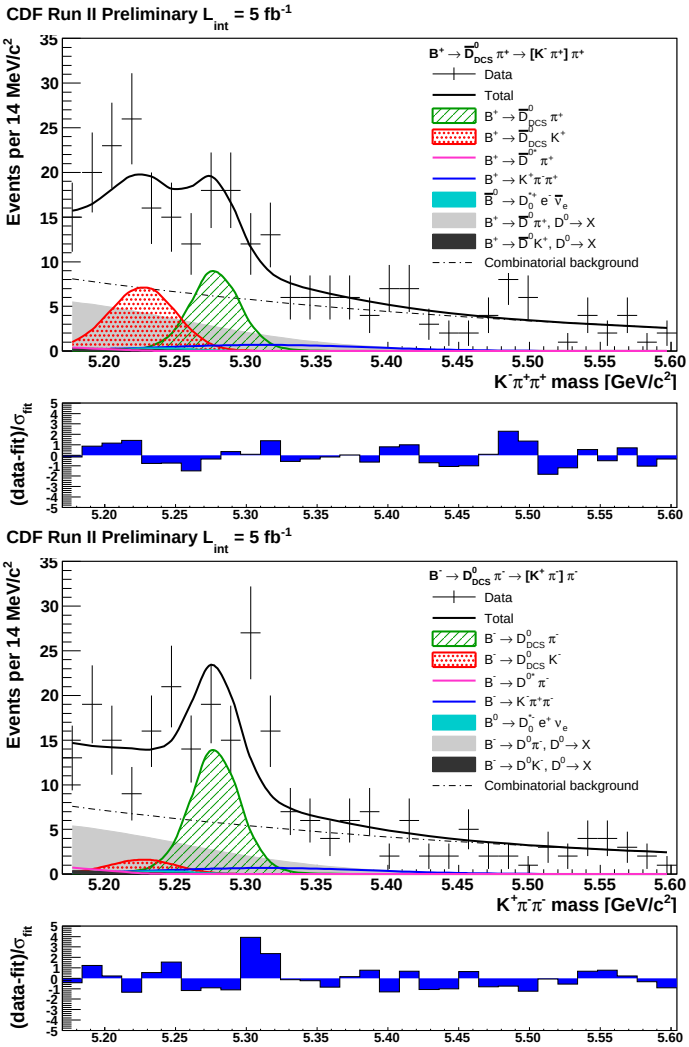


FIG. 8. Fit projection onto the $m_{D^0\pi}$ variable for the doubly Cabibbo-suppressed mode, positive charges (top) and negative charges (bottom).

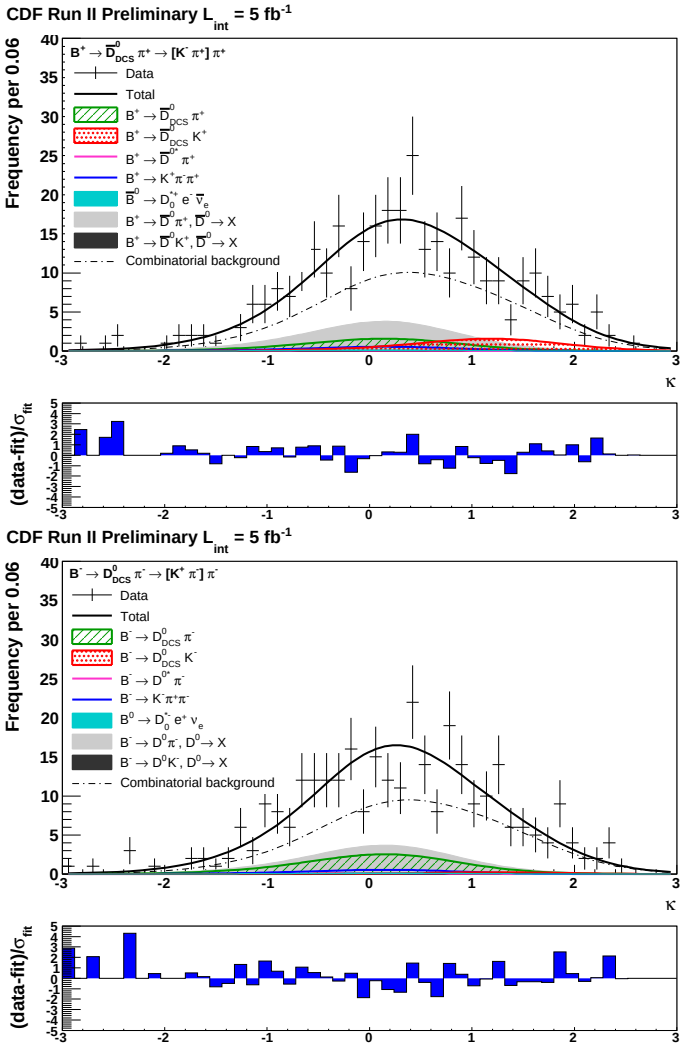


FIG. 9. Fit projection onto the $\kappa$ variable for the doubly Cabibbo-suppressed mode, positive charges (top) and negative charges (bottom).

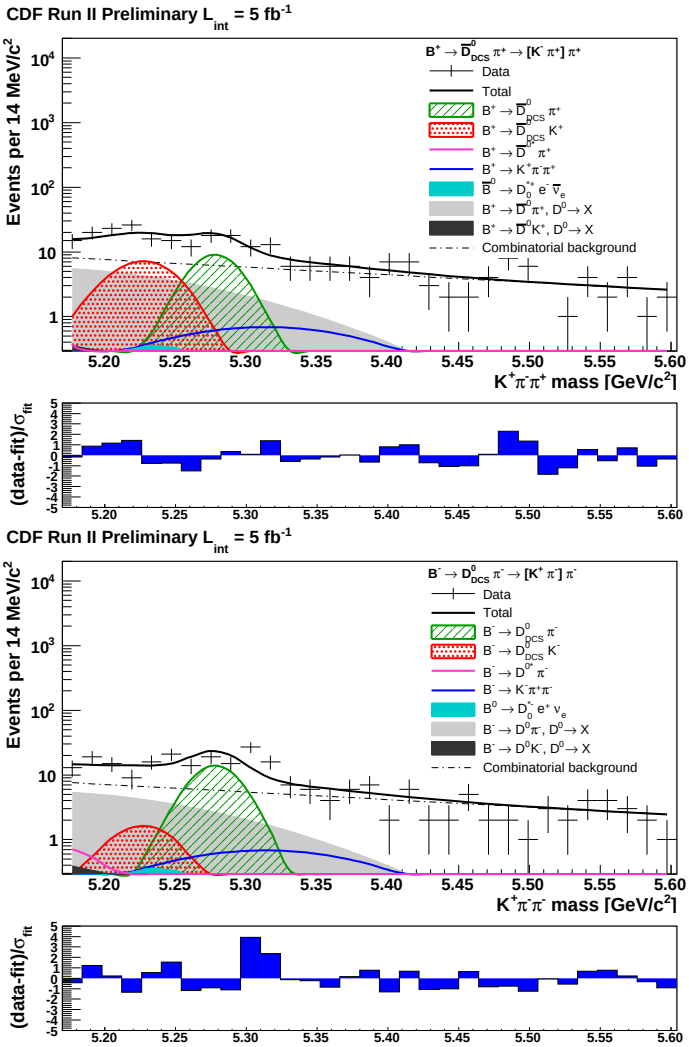


FIG. 10. Fit projection (logarithmic scale) onto the $m_{D^0\pi}$ variable for the doubly Cabibbo-suppressed mode, positive charges (top) and negative charges (bottom). Backgrounds contributions are more evident.

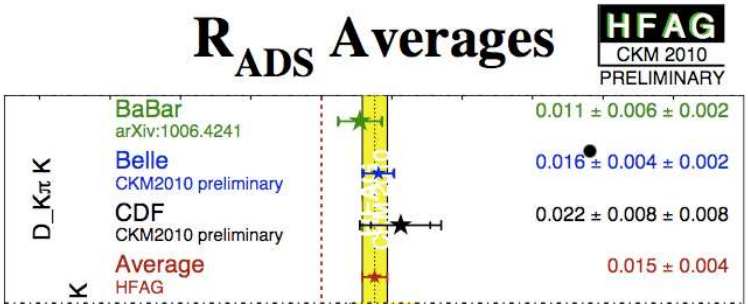


FIG. 11. $R_{ADS}(K)$ measurement. Comparison with other experiments.

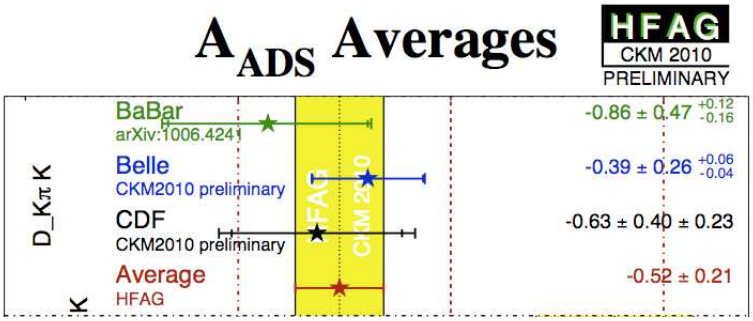


FIG. 12. $A_{ADS}(K)$ measurement. Comparison with other experiments.

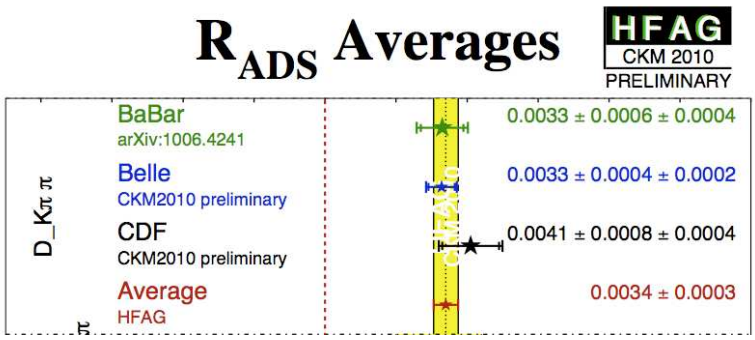


FIG. 13. $R_{ADS}(\pi)$ measurement. Comparison with other experiments.

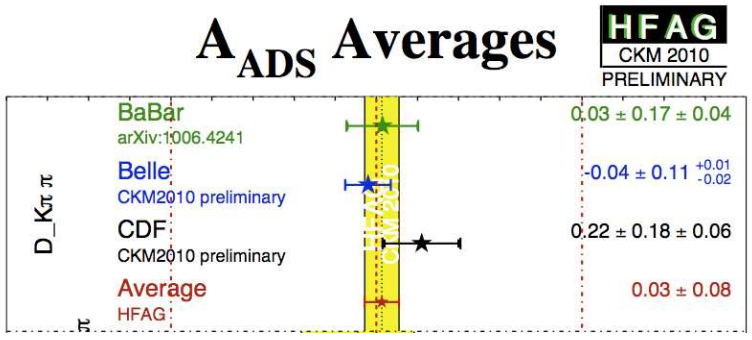


FIG. 14. $A_{ADS}(\pi)$ measurement. Comparison with other experiments.